Chapter 11

Results

11.1 Finite-size scaling methodology

Finite-size scaling takes the form of a hypothesis, or rather a set of hypotheses, which is tested against the data. See [PV] for an excellent survey of techniques; see section 11.2 for a derivation of the formulas.

We have an infinite-volume random variable $S(T)$, e.g. any of the order parameters defined in section 3.7. The finite-volume quantity is $S_L(T)$. Define $t = (T - T_c)/T_c$. Examine, say, $0.99 < t < 1.01$. The first hypothesis is that the correlation length $\xi(T)$ follows a power law

$$\xi(T) \sim |t|^{-\nu}, \quad T \to T_c$$

For the infinite-volume quantity, we also expect a power-law behavior

$$S(T) \sim t^\rho, (-t)^\rho, \quad \text{or} \quad |t|^\rho, \quad \text{i.e.} \quad \xi^{-\rho/\nu}.$$

(The domain of validity is $t < 0$ or $t > 0$ depending on whether the order parameter S is left-sided or right-sided, respectively.) One moreover hypothesizes that for T near T_c, $S_L(T)$ and $S(T)$ are related by a *universal function* Q_S which depends on T only through the ratio L/ξ:

$$S_L(T) = L^{-\rho/\nu} Q_S(L^{1/\nu} t) \sim L^{-\rho/\nu} Q_S((L/\xi)^{1/\nu}). \tag{11.1.1}$$

The flow of data and respective uncertainties are as follows:

- Markov chain Monte Carlo simulations, with error bars determined using the method of integrated autocorrelation time (see [Berg] and our appendix B), yield $S_L(T, \alpha)$ data points. There are five order parameters S, six values of L (30, 40, 50, 60, 70, 80), nine values of α, and a few dozen values of T for each α.

- For each S, L, and α, we use $S_L(T, \alpha)$ values for all available values of T and α to estimate [1] $\hat{\rho}_S(L)$. (Critical exponents are assumed to be independent of α for small α, or with weak enough dependence on α that that dependence is lost in the noise.) Error bars may be propagated from the MCMC simulations, or computed from regression uncertainties.

[1] We use the statistics convention wherein $\hat{\rho}$ is an experimental estimator for the exact (but unknown) value ρ.

- Extrapolating $\hat{\rho}_S(L)$ in $L \to \infty$ results in the five estimated critical exponents $\hat{\rho}_S$. Uncertainties are computed from the regression analysis.
- Once the critical exponents have been estimated, we obtain $\hat{T}_{c,S}(\alpha)$ for each of the five order parameters S and for each α. Uncertainties are computed by visual inspection of the crossing plots discussed in section 11.5.
- Once the critical exponents and T_c have been estimated, one should be able to obtain plots of the universal function Q_S which is, up to sampling variability, independent of L, T, and α. This verifies that the finite-size-scaling hypothesis was the correct approach to use.
- The shift in reduced critical temperature is as in equation (2.3.1). Error bars are computed from regression uncertainties.

11.2 Derivation of finite-size scaling

A clear explanation is found in on-line notes of Claudia Brüns of the Argelander Institute for Astronomy of the University of Bonn. (We are unwilling to provide a bibliographic reference to an internet address, which may change in the future. Nonetheless, we feel compelled to acknowledge the author to whom this expalanation is due.) Those notes are are reproduced essentially verbatim in this section, except for change of notation.

For T away from T_c, $\xi \ll L$ and so $S_L(T)$ is not affected by lattice size. The finite-volume quantity $S_L(T)$ corresponds to the infinite-volume quantity $S_\infty(T)$, and we know $S_\infty(T) \propto \xi^{-\rho/\nu}$ as discussed in the previous section. For T near T_c, on the other hand, the correlation length ξ approaches the system size L so $S_L(T) \propto \xi^{-\rho/\nu} \approx L^{-\rho/\nu}$. As well, $S_L(T)$ differs significantly from $S_\infty(T)$ via the constant of proportionality. Combining these two regimes into a single expression gives

$$S_L(T) = \xi^{-\rho/\nu} R_S(L/\xi) \tag{11.2.1}$$

where

$$R_S(L/\xi) \propto \begin{cases} \text{constant}, & \xi \ll L \\ (L/\xi)^{-\rho/\nu}, & \xi \to L. \end{cases} \tag{11.2.2}$$

The infinite-volume correlation length $\xi = \xi_\infty(T)$ is unknown, so we define a scaling function Q_S to get rid of it:

$$Q_S(L/\xi) = (L/\xi)^\rho R_S((L/\xi)^\nu), \tag{11.2.3}$$

i.e.

$$R_S(L/\xi) = (L/\xi)^{-\rho/\nu} Q_S((L/\xi)^{1/\nu}). \tag{11.2.4}$$

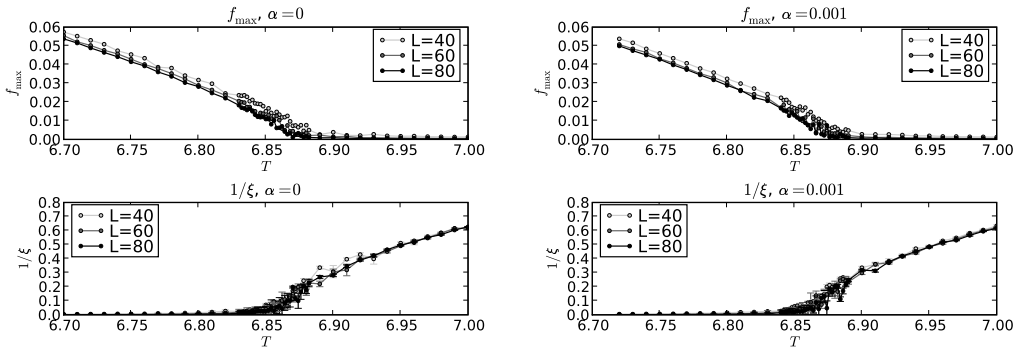

FIGURE 11.1. Order parameters $f_{\max}$ and $1/\xi$ for $L = 40, 60, 80$ and $\alpha = 0$ and 0.001. The remaining order parameters f_S, f_W, and f_I behave similarly to $f_{\max}$ but with not all with the same critical exponents.

The scaling function Q_S is finite for $\xi \to L$:

$$Q_S(L/\xi) = (L/\xi)^\rho R_S((L/\xi)^\nu) \tag{11.2.5}$$

$$Q_S(L/\xi) \propto (L/\xi)^\rho \cdot ((L/\xi)^\nu)^{-\rho/\nu} = 1. \tag{11.2.6}$$

Placing equation (11.2.4) into equation (11.2.1) yields

$$S_L(T) = \xi^{-\rho/\nu}(L/\xi)^{-\rho/\nu} \cdot Q_S((L/\xi)^{1/\nu}) \tag{11.2.7}$$

$$= L^{-\rho/\nu} Q_S(L^{1/\nu}\xi^{-1/\nu}) \tag{11.2.8}$$

$$= L^{-\rho/\nu} Q_S(L^{1/\nu} t). \tag{11.2.9}$$

11.3 Determination of L-dependent critical exponents

For each of order parameter S, interaction parameter α, and box length L, we examine all $S(L, T, \alpha)$ data for which $S > \varepsilon$, with ε taken from the plots to ensure that we examine the portions of the curves corresponding to non-zero order parameter in the infinite limit (see figure 11.1). For $1/\xi$, this means $T > T_c$; for the other four order parameters, this means $T < T_c$. From plots such as those in figure 11.1, we choose ε to be 0.1 for $1/\xi$, 0.01 for $f_{\max}$, 0.01 for f_I, 0.05 for f_S, and 0.01 for f_W. For each S, α, and L, we then apply linear regression to $S(L, T)^{1/\rho_S}$ for varying ρ_S. We find $\hat{\rho}_S(L)$ which optimizes the correlation coefficient [Young] of the linear regression. Results are shown in figure 11.2. Given $\hat{\rho}_S(L)$ along with its corresponding linear-regression parameters $\hat{m}$ and $\hat{b}$, we may plot a power-law fit to the simulational data. One such comparison plot is shown in figure 11.3.

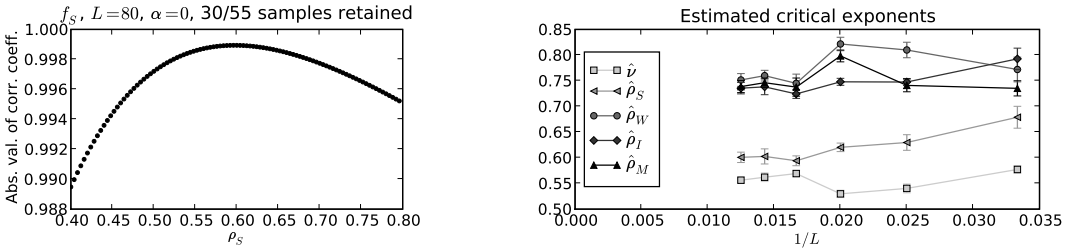

FIGURE 11.2. On the left: determination of critical exponent $\hat{\rho}_S(L, \alpha)$ for order parameter f_S, as the value which minimizes linear-regression error for $S_L(T, \alpha)^{1/\rho}$. Visually, one sees $\hat{\rho}_S(L = 80, \alpha = 0.0) \approx 0.59$. On the right: estimated critical exponents for $L = 30, 40, 50, 60, 70, 80$.

α	Mean	Std.err.	Count
0.000	0.6242981	0.0000897	78
0.0001	0.6243312	0.0001079	78
0.0002	0.6245691	0.0000921	72
0.0005	0.6245402	0.0001062	66
0.0008	0.6244347	0.0000856	72
0.001	0.6244779	0.0001020	60
0.002	0.6246345	0.0001154	42
0.003	0.6245906	0.0001559	48
0.004	0.6245966	0.0001964	42

TABLE 11.1. $f_{\max}/f_I$ as a function of α. An upward trend is visible, but it is not pronounced.

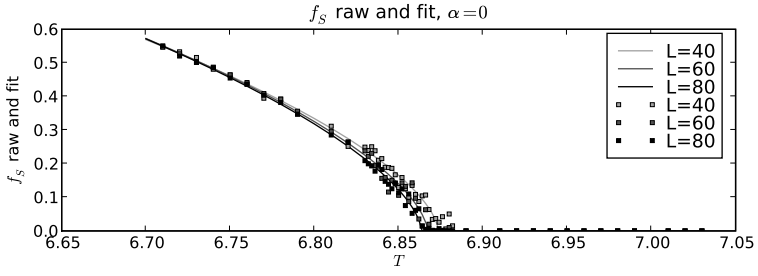

FIGURE 11.3. Power-law fit vs. raw simulational data for order parameter f_S, $\alpha = 0$.

$\hat{\nu}$	0.5559	$\pm$ 0.0037
$\hat{\rho}_S$	0.6201	$\pm$ 0.0065
$\hat{\rho}_W$	0.7750	$\pm$ 0.0073
$\hat{\rho}_I$	0.7451	$\pm$ 0.0052
$\hat{\rho}_M$	0.7486	$\pm$ 0.0059

TABLE 11.2. Extrapolated estimates of the infinite-volume critical exponents, found from the vertical intercept of figure 11.2.

11.4 Extrapolation of critical exponents for the infinite-volume limit

Next, for each S, given estimates $\hat{\rho}_S(L)$ for increasing values of L, we plot $\hat{\rho}_S(L)$ versus $1/L$. The vertical intercept of this plot estimates the infinite-volume exponent $\hat{\rho}_S(\alpha)$. (See figure 11.2.) Results are shown in table 11.2.

11.5 Determination of critical temperature

Given the above estimators of the critical exponents, the *crossing method* [PV] estimates $T_c(\alpha)$. Namely, we plot $L^{\hat{\rho}/\hat{\nu}} S_L(T)$ as a function of T. At $T = T_c$ we have $t = 0$ and $L^{\rho/\nu} S_L(T) = Q_S(0)$, regardless of L (equation (11.1.1)). Thus, these curves will cross (approximately, due to sampling variability) at $T = T_c$. If they do not, the finite-size-scaling hypothesis is not verified. (Note in particular that for order parameter $1/\xi$ whose critical exponent is ν, we apply the crossing method to $LS_L(T)$ as a function of T: thus, the $T_c(\alpha)$ estimate using $1/\xi$ is independent of $\hat{\nu}$.) See for example figure 11.4. Results are in table 11.3 and figure 11.6

Using order parameters f_S and f_W, which depend on winding phenomena, one does not see clear crossing behavior. We suggest that either this is related to the even-winding-number issue discussed in section 5.4, or f_S and f_W are not good order parameters for this model. We suspect the former; in every manner except this crossing issue, f_S and f_W behave as expected. (In the absence of clear crossing behavior for f_S and f_W, for the sake of discussion we nonetheless provide best visual estimates for $\hat{T}_c(\alpha)$ for f_S and f_W. These will not be used for further analysis toward our final result.)

11.6 Verification of finite-size-scaling hypothesis

Now that we have estimated ρ_S, ν, and $T_c(\alpha)$ for each of the five order parameters S, we may plot $L^{\rho_S/\nu} S_L(T, \alpha)$ as a function of $L^{1/\nu} t$. This is a plot of the scaling function Q_S. If the hypothesis is correct, the curves for all L should coincide, or collapse, to within sampling error — which they do (e.g. figure 11.5).

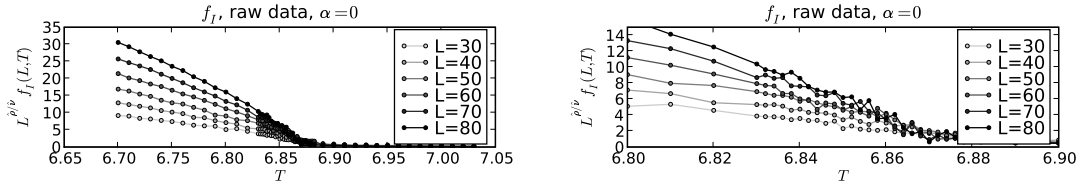

FIGURE 11.4. The crossing method to estimate $T_c(\alpha)$ for order parameter f_I, with $\hat{\rho}$ and $\hat{\nu}$ as above: $T_c(\alpha)$ corresponds to the horizontal coordinate of the intersection point of the plots. The upper-right-hand plot is a close-up of the upper-left-hand plot. Order parameters f_S and f_W, which depend on winding phenomena, do not exhibit clear crossing behavior.

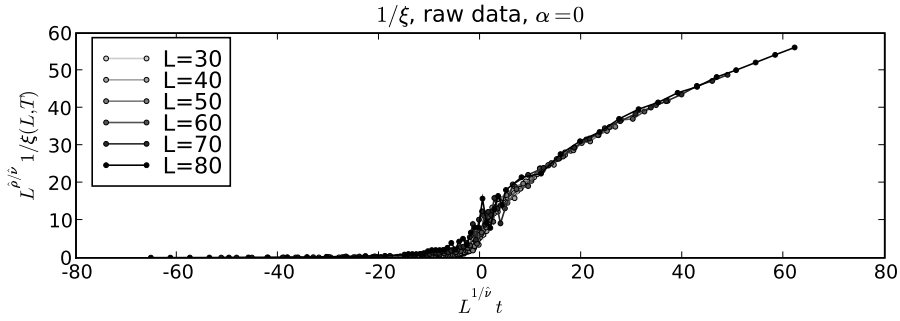

FIGURE 11.5. Collapse plot for order parameter $1/\xi$.

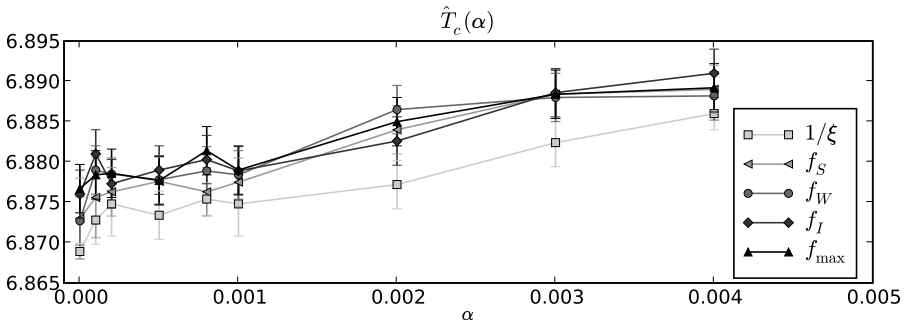

FIGURE 11.6. Critical temperature as function of α.

11.7 Determination of the shift in critical temperature

As discussed in section 2.5, we are seeking a linear relationship between $\Delta T_c(\alpha)$ and α, with constant c. This can be visualized in figure 11.7, which is obtained from the $T_{c,S}(\alpha)$ data of figure 11.6 using equation (2.3.1). We start with all the $(\alpha, \Delta T_c(\alpha))$ data points from section 11.5. We omit values obtained using f_S and f_W, due to the aforemention lack of crossing behavior. We also omit values obtained using $\alpha = 0.004$, since the critical-temperature plots of figure 11.6 suggests that this starts to exceed the domain of linear approximation. We perform a linear regression with error bars [Young] on the $(\alpha, \Delta T_c(\alpha))$ data points. We use a slope-only fit, rather than a slope-intercept fit, since $\Delta T_c(\alpha)$ has zero intercept by its very definition. We find

$$c = 0.618 \pm 0.086 \text{ (2 } \sigma \text{ error bar).}$$

Within experimental uncertainty, this result, for points on the lattice with Ewens cycle-weights, matches the c value of equation (2.5.3) for point positions varying on the continuum with decaying-cycle-weight interactions.

11.8 Constancy of the macroscopic-cycle quotient

As discussed in section 2.5, we hypothesize that the macroscopic-cycle quotient $f_{\max}/f_I$ in the infinite-volume limit is dependent on α but is constant in T where it is defined, i.e. for $T < T_c$ since $f_I = 0$ for $T > T_c$. This may be visualized by comparing figures such as 2.4: one sees that $f_{\max}$ and f_I appear to have the same critical exponent. Alternatively, one may plot the ratio $f_{\max}/f_I$ (figure 11.8). In the infinite-volume limit, f_I is zero for $T > T_c$ and so we are interested only in the values of the quotient for $T < T_c$. In that region, the quotient does indeed appear to be constant in T.

We test this constancy hypothesis as follows. The respective critical exponents are ρ_M and ρ_I. The estimators are $\hat{\rho}_M$ and $\hat{\rho}_I$, computed by averaging over several

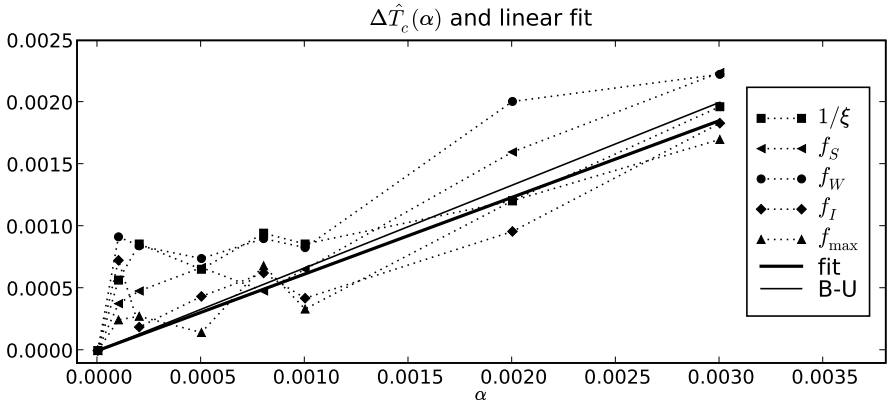

FIGURE 11.7. Shift in critical temperature, and linear fit, as function of α. Recall from equation (2.3.1) that $\Delta T_c(\alpha) = \frac{T_c(\alpha) - T_c(0)}{T_c(0)}$. Order parameters f_S and f_W were omitted from the fit, due to lack of crossing behavior; $\alpha = 0.004$ was omitted due to onset of curvature of $T_c(\alpha)$. The heavy solid line shows a linear fit with empirically determined constant of proportionality; the lighter solid line is the comparison value of Betz and Ueltschi (slope 2/3) for decaying cycle weights and continuum point positions.

α	Using $1/\xi$	Using f_S	Using f_W	Using f_I	Using $f_{\max}$
0.000	6.8689	6.8730	6.8727	6.8760	6.8767
0.0001	6.8728	6.8756	6.8790	6.8810	6.8784
0.0002	6.8748	6.8763	6.8785	6.8773	6.8786
0.0005	6.8734	6.8776	6.8778	6.8790	6.8777
0.0008	6.8754	6.8763	6.8789	6.8803	6.8814
0.001	6.8748	6.8775	6.8784	6.8789	6.8790
0.002	6.8772	6.8840	6.8865	6.8826	6.8850
0.003	6.8824	6.8884	6.8880	6.8886	6.8884
0.004	6.8860	6.8890	6.8882	6.8910	6.8892

TABLE 11.3. Critical temperature as a function of α. All values have error bars of approximately 0.003.

different values of L and α as described in section 11.4. Treating these estimators as normally distributed (as justified by the raw data), we obtain the standard deviations of the $\hat{\rho}_{M,I}(L,\alpha)$ samples, along with the standard deviations of the means $\hat{\rho}_{M,I}$:

$$\begin{aligned} \hat{\rho}_M &= 0.7482 & \hat{\rho}_I &= 0.7445 \\ s_M &= 0.0428 & s_I &= 0.0374 \\ n_M &= 50 & n_I &= 50 \\ s_M/\sqrt{n_M} &= 0.006059 & s_I/\sqrt{n_I} &= 0.005295. \end{aligned}$$

The difference $\hat{\rho}_M - \hat{\rho}_I$ is also normally distributed about the true mean $\rho_M - \rho_I$, but $\hat{\rho}_M$ and $\hat{\rho}_I$ are not independent since they are sample means of random variables computed from the same Markov chain Monte Carlo sequence of permutations. Thus we use

$$\mathrm{Var}(\hat{\rho}_M - \hat{\rho}_I) = \mathrm{Var}(\hat{\rho}_M) + \mathrm{Var}(\hat{\rho}_I) - 2\mathrm{Cov}(\hat{\rho}_M, \hat{\rho}_I).$$

Computing the sample covariance of the $\hat{\rho}_M(L,\alpha)$ and $\hat{\rho}_I(L,\alpha)$ data series, we obtain the covariance and resulting standard error s_d of the difference

$$\mathrm{Cov}(\hat{\rho}_M, \hat{\rho}_I) = 0.0004 \qquad s_d/\sqrt{n} = 0.0070.$$

Normalizing, we find

$$\hat{\rho}_M - \hat{\rho}_I = 0.0037 \qquad \frac{\hat{\rho}_M - \hat{\rho}_I}{s_d/\sqrt{n}} = \frac{0.0037}{0.0070} = 0.5293.$$

We hypothesize $\rho_M - \rho_I = 0$; the estimated value $\hat{\rho}_M - \hat{\rho}_I$ lies comfortably within a standard deviation of this. We note, moreover, that the value of $f_{\max}/f_I$, while constant in T, trends upward with α (see table 11.1 and figure 11.9). This merits further investigation.

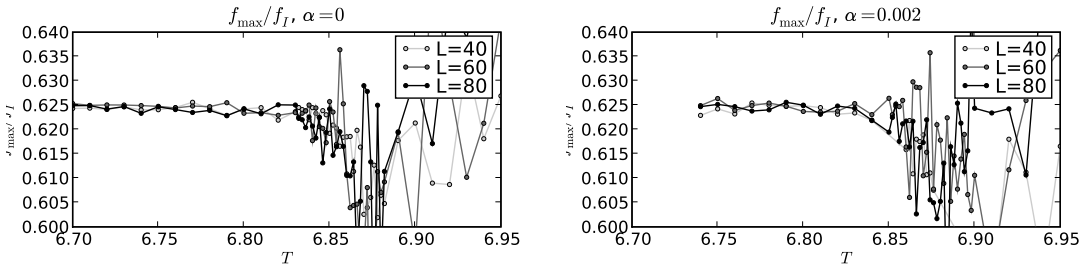

FIGURE 11.8. Macroscopic-cycle quotient $f_{\max}/f_I$ for $\alpha = 0, 0.002$.

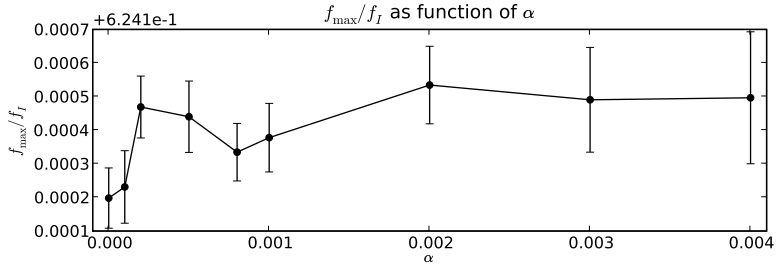

FIGURE 11.9. $f_{\max}/f_I$ as a function of α.

11.9 Conclusions

(1) For annealed point positions, equation (2.5.2) gives $T_c(0) \approx 6.625$. Our result $T_c(0) = 6.873 \pm 0.006$ (2 σ error bar) unambiguously shows that the lattice structure modifies the critical temperature, even in the non-interacting ($\alpha = 0$) case.

(2) As detailed in section 11.7, we find that the reduced shift in critical temperature as a function of interaction parameter α is

$$\Delta T_c(\alpha) \approx \frac{T_c(\alpha) - T_c(0)}{T_c(0)} = c\alpha$$

with

$$c = 0.618 \pm 0.086 \text{ (2 } \sigma \text{ error bar)}.$$

This is compatible (section 2.5) with the related result of [BU08]. Even though the lattice structure changes the critical temperature (conclusion 1), the *shift* in critical temperature is unaffected.

(3) As described in section 2.4, Shepp and Lloyd [SL] find that $\mathbb{E}[\ell_{\max}]/N \approx 0.6243$ for uniform-random (non-spatial) permutations. For spatial permutations, we define a macroscopic-cycle quotient $\mathbb{E}[\ell_{\max}]/Nf_I$ which is the ratio of mean maximum cycle length as a fraction of the number of sites in long cycles. Our result (table 11.1 and figure 11.9) is compatible with that of Shepp and Lloyd for the non-interacting case, with an increase which appears to be linear as a function of interaction parameter α.

(4) We proved correctness for the pre-existing SO algorithm [GRU]; we invented the SAR, band-update, and worm algorithms, and proved them correct. The band-update algorithm suffers from a too-low acceptance probability; the worm algorithm suffers from a too-long stopping time; the SO algorithm prohibits (with very high probability) non-zero winding numbers. The SAR algorithm is our current best option, even though it only permits even winding numbers. Solving the deficiencies of the band-update or worm algorithms would be worth the effort.

(5) The order parameter $1/\xi$ is the most convenient to use for our problem: in the finite-size-scaling analysis, the crossings are independent of estimated critical exponent $\hat{\nu}$. The order parameters f_I and $f_{\max}$ are second-most convenient; one must estimate their critical exponents, but they are usable. The order parameters f_S and f_W, which depend on winding phenomena, do not pass the finite-size-scaling hypothesis. Either they are not good order parameters for the model of random spatial permutations, or they would benefit from a full-winding-number algorithm as discussed in the previous paragraph.